Smart design of free-standing ultrathin Co-Co(OH)$_2$ composite nanoflakes on 3D nickel foam for high-performance electrochemical capacitors

**Zheyin Yu, Zhenxiang Cheng,* Siti Rohana Majid,
Zhixin Tai, Xiaolin Wang, and Shixue Dou**
Institute for Superconducting and Electronic Materials, University of Wollongong, North Wollongong, NSW 2500, Australia. E-mail: cheng@uow.edu.au; Fax: +61-2-42215731; Tel: +61-2-42981406

Experimental

Material synthesis

All reagents used in this experiment were of analytical grade without further purification. Before electrodeposition, the nickel foam was carefully cleaned with acetone and absolute ethanol, respectively, and then rinsed with pure water. The electrolyte in the experiment was prepared from deionized water and analytical grade chemicals, which consisted of 1 M $CoCl_2 \cdot 6H_2O$, 0.5 M H_3BO_3, and 2 M ethylenediamine dihydrochloride. In addition, the pH value of the electrolyte solution was adjusted to 4.0 using 10% HCl and 10% NH_4OH solutions. The electrolyte temperature was kept at 40°C. A Pt plate was used as the anode, and a piece of nickel foam was used as the substrate for electrodeposition. The cathode current density was 10 A/dm^2. The synthesis of Co-Co(OH)$_2$ composite nanoflakes (CCCNs) may comprise the electrodeposition process via Reaction (1) and the subsequent oxidation process in electrolyte via Reaction (2). It should be noted that surface metallic Co will be unavoidably oxidized by water into Co(OH)$_2$ after electrodeposition[16]. The process for the synthesis of CCCNs is illustrated in Fig. S1.

$$Co^{2+}_{(aq)} + 2e \rightarrow Co_{(s)} \quad (1)$$

$$Co_{(s)} + 2H_2O \rightarrow Co(OH)_2 \cdot H_2O + H^+ + e^- \quad (2)$$

The above two-step reaction is different from the generally reported fabrication of Co(OH)$_2$ in Co(NO)$_3$ solution, which involves the reduction of NO_3^- to generate OH^- species via Reaction (3) , which, in turn, give rise to the formation of pure Co(OH)$_2$ via Reaction (4)[14].

$$NO_3^- + 7H_2O + 8e^- \rightarrow NH_4^+ + 10OH^- \quad (3)$$

$$Co^{2+} + 2OH^- \rightarrow Co(OH)_2 \quad (4)$$

After electrodeposition, the nickel foam was carefully rinsed with deionized water several times, and then dried in a 60 ºC oven for 8 hours. The mass of the CCCNs was estimated by weighing the mass before and after the electrodeposition process, after drying, with an electronic balance (model MSA125P-100-DI, 0.01 mg resolution, Sartorius, Germany).

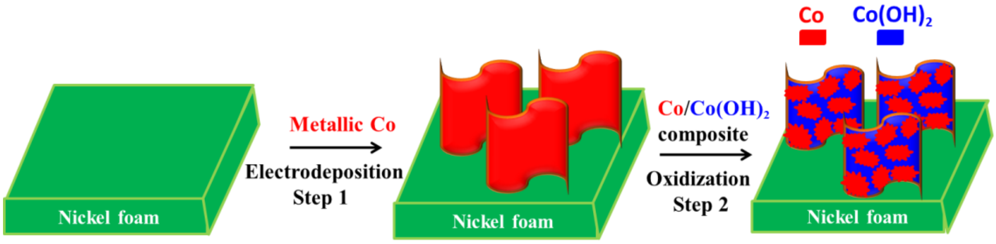

Figure S1 Schematic illustration of the synthesis of Co-$Co(OH)_2$ composite nanoflakes on 3D nickel foam.

Structural characterization

X-ray photoelectron spectroscopy (XPS) was conducted using a SPECS PHOIBOS 100 Analyser installed in a high-vacuum chamber with the base pressure below 10^{-8} mbar. X-ray excitation was provided by Al Kα radiation with photon energy hv = 1486.6 eV at the high voltage of 12 kV and power of 120 W. The XPS binding energy spectra were collected with pass energy of 20 eV in the fixed analyzer transmission mode. Wide-angle (10°–100°) powder X-ray diffraction (XRD) was carried out using a polycrystalline X-ray diffractometer (RIGAKU, D/MAX 2550 VB/PC, 40 kV/200 mA, λ = 1.5406 Å). The morphologies were investigated by field-emission scanning electron microscopy (FESEM; JEOL JSM-7500FA) and transmission electron microscopy (TEM; JEOL ARM200F). Before FESEM testing, a 5 nm Pt coating was sputtered onto the sample in order to obtain clear images.

Electrochemical measurements

The electrochemical performance of the as-prepared electrode was measured using cyclic voltammetry (CV), galvanostatic charge/discharge (GCD) testing, and electrochemical impedance spectroscopy (EIS) on an electrochemical workstation (CHI 660c, Shanghai CH Instrument Company, China), with a typical three-compartment cell at ambient temperature. In the three-compartment cell, the as-prepared free-standing electrode was used for the working electrode, platinum plate (2×2 cm^2) was used for the counter electrode, and saturated calomel electrode (SCE) was used for the reference electrode. The electrolyte was

2 M KOH solution. EIS measurements were performed by applying an AC voltage with 5 mV amplitude in the frequency range from 0.01 Hz to 100 kHz. Cycling stability measurements were carried out on a Land battery testing system.

The specific capacitance (C_{sp}) was estimated from the CV curves according to the following Equation (5):

$$C_{sp} = (|Q_-| + Q_+) / (2m \times \Delta V \times v) \tag{5}$$

where Q_- and Q_+ are the cathodic integrated charges and the anodic integrated charges, respectively. m is the mass (g) of the CCCNs, ΔV is the potential window (0.55 V), and v is the scan rate (V/s).

The specific capacitance was also estimated from the charge/discharge curves according to the following Equation (6):

$$C_{sp} = I \times t / (m \times \Delta V) \tag{6}$$

where I is the current (A) during the charging/discharging process, t is the discharging time (s) in each segment, ΔV is the potential window (0.55 V), and m is the mass (g) of the CCCNs.

The specific energy density, E (Wh/kg), and specific power density, P (W/kg), were defined according to the following Equations (7) and (8), respectively:

$$E = C_{sp} \times \Delta V^2 / 7.2 \tag{7}$$

$$P = E \times 3600 / t \tag{8}$$

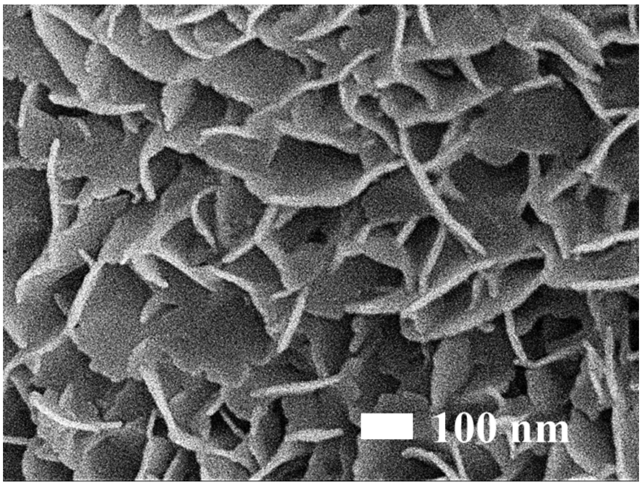

Figure S2 SEM image of CCCNs.

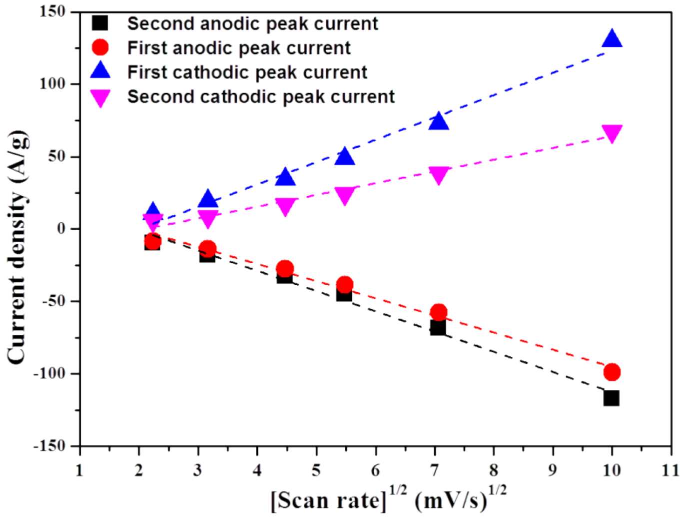

Figure S3 Linear relationship between cathodic peak current or anodic peak current and the square root of the scan rate.

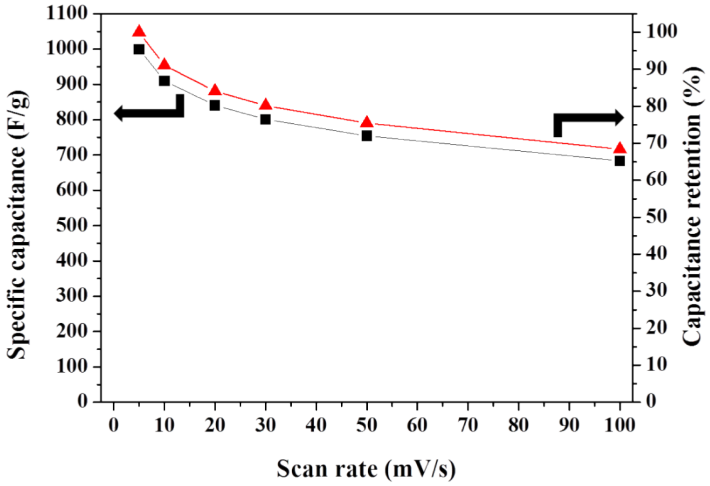

Figure S4 Variation of the specific capacitance and the capacitance retention with the scan rate.

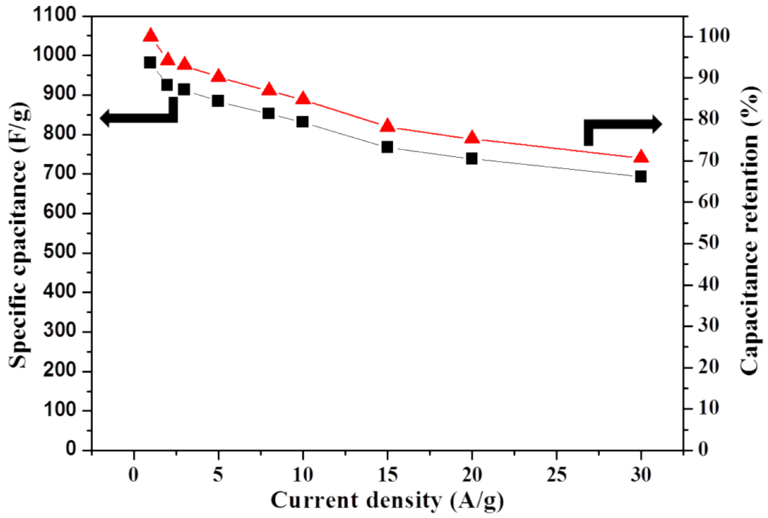

Figure S5 Variation of the specific capacitance and capacitance retention with current density.

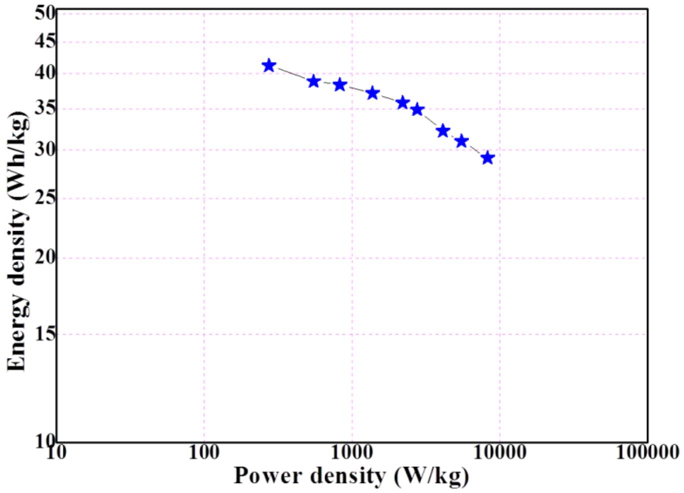

Figure S6 Ragone plot of CCCNs.

Table S7 Comparison of the electrochemical performance in previous reports on $Co(OH)_2$ materials in ECs with the $Co\text{-}Co(OH)_2$ composite nanoflakes presented here.

Material	Preparation method	Specific capacitance (F/g)	Rate performance	Capacitance retention	Ref.
$Co(OH)_2$ nanosheets	Electrodeposition	604 (5 mV/s)	75% (50 mV/s)	76% (500 cycles)	14
$Co(OH)_2$ nanowires	Electrodeposition	1180 (4 A/g)	No data	52% (1000 cycles)	S1
$Co(OH)_2$/ITO nanowires	Electrodeposition	2052 (1 A/g)	74% (20 A/g)	91.59% (1200cycles)	S2
$Co(OH)_2$ nanosheets	Electrodeposition	881 (1 A/g)	87% (10 A/g)	91% (2000 cycles)	S3
$Co(OH)_2$ nanosheets	Electrodeposition	1084 (4 A/g)	67% (48 A/g)	95% (500 cycles)	S4
$Co(OH)_2$ porous film	Electrodeposition	1473 (2 A/g)	67% (32 A/g)	88% (1000 cycles)	S5
$Co(OH)_2$ nanowires	Dual-template electrodeposition	480 (1 A/g)	81% (20 A/g)	No data	S6
$Co(OH)_2$ nanoflowers	Chemical precipitation	416 (1 A/g)	77% (5 A/g)	93% (500 cycles)	S7
$Co(OH)_2$ nanocones	Hydrothermal	562 (2 A/g)	67% (22 A/g)	88% (3000 cycles)	S8
$Co(OH)_2$ nanoflakes	Chemical precipitation	559 (5 mV/s)	81% (50mV/s)	81% (2000 cycles)	S9
$Co(OH)_2$ nanorods	Chemical bath deposition	1139 (5 A/g)	33% (25 A/g)	74% (1000 cycles)	S10
$Co(OH)_2/TiO_2$ nanowalls	Electrodeposition	498 (5 mV/s)	51% (125 mV/s)	82.5% (5000 cycles)	S11
$Co(OH)_2$/graphene film	Electrodeposition	693 (2 A/g)	73% (32 A/g)	91.1% (3000 cycles)	S12
$Co(OH)_2$ nanowires	Hydrothermal	358 (0.5 A/g)	90% (10 A/g)	86.3% (5000 cycles)	S13
$Co(OH)_2$ nanocones	Chemical precipitation	1055 (1 A/g)	28% (15 A/g)	95% (2000 cycles)	S14
$Co\text{-}Co(OH)_2$ composite nanoflakes	Electrodeposition	1000 (5 mV/s) or 980 (1 A/g)	70.71%(100 mV/s) or 68.40% (30 A/g)	91% (5000 cycles, 100% capacitance retention in previous 3100 cycles)	This work

References:

S1 T. Xue and J.-M. Lee, *Journal of Power Sources*, 2014, **245**, 194.

S2 D. Tai Dam and J.-M. Lee, *Nano Energy*, 2013, **2**, 1186.

S3 V. Gupta, T. Kusahara, H. Toyama, S. Gupta and N. Miura, *Electrochemistry Communications*, 2007, **9**, 2315.

S4 W.-j. Zhou, J. Zhang, T. Xue, D.-d. Zhao and H.-l. Li, *Journal of Materials Chemistry*, 2008, **18**, 905.

S5 L.-B. Kong, M.-C. Liu, J.-W. Lang, M. Liu, Y.-C. Luo and L. Kang, *Journal of Solid State Electrochemistry*, 2010, **15**, 571.

S6 T. Xue, X. Wang and J.-M. Lee, *Journal of Power Sources*, 2012, **201**, 382.

S7 C. Mondal, M. Ganguly, P. K. Manna, S. M. Yusuf and T. Pal, *Langmuir*, 2013, **29**, 9179.

S8 F. Cao, G. X. Pan, P. S. Tang and H. F. Chen, *Journal of Power Sources*, 2012, **216**, 395.

S9 Y. K. Kim, S. I. Cha and S. H. Hong, *Journal of Materials Chemistry A*, 2013, **1**, 9802.

S10 U. M. Patil, S. C. Lee, J. S. Sohn, S. B. Kulkarni, K. V. Gurav, J. H. Kim, J. H. Kim, S. Lee and S. C. Jun, *Electrochimica Acta*, 2014, **129**, 334.

S11 A. Ramadoss and S. J. Kim, *Electrochimica Acta*, 2014, **136**, 105.

S12 C. Zhao, X. Wang, S. Wang, Y. Wang, Y. Zhao and W. Zheng, *International Journal of Hydrogen Energy*, 2012, **37**, 11846.

S13 Y. Tang, Y. Liu, S. Yu, S. Mu, S. Xiao, Y. Zhao and F. Gao, *Journal of Power Sources*, 2014, **256**, 160.

S14 L. Wang, Z. H. Dong, Z. G. Wang, F. X. Zhang and J. Jin, *Advanced Functional Materials*, 2013, **23**, 2758.